Oscillatory instability in slow crack propagation in rubber under large deformation

Daiki Endo,[1] Katsuhiko Sato,[2] and Yoshinori Hayakawa[3]
[1]*Department of Physics, Tohoku University, Sendai 980-8578, Japan*
[2]*RIKEN Center for Developmental Biology, Kobe 650-0047, Japan*
[3]*Center for Information Technology in Education, Tohoku University, Sendai 980-8576, Japan*
(Received 7 November 2011; published 11 July 2012)

We performed experiments to investigate slow fracture in thin rubber films under uniaxial tension using high-viscosity oils. In this system we observed an oscillating instability in slowly propagating cracks for small applied strains. The transition between oscillatory and straight patterns occurred near the characteristic strain at which rubber exhibits a nonlinear stress-strain relation. This suggests that nonlinear elasticity plays an important role in the formation of the observed pattern. This was confirmed by numerical simulation for neo-Hookean and linear elasticity models.

DOI: 10.1103/PhysRevE.86.016106 PACS number(s): 46.50.+a, 81.05.Lg, 83.60.Uv, 89.75.Kd

I. INTRODUCTION

On propagating cracks, various type of instabilities and qualitative changes of crack patterns accompanied by the instabilities are known. For example, when a rubber balloon is ruptured, oscillatory crack patterns on a macroscopic scale are observed quite consistently [1]. This phenomenon has attracted much interest from researchers. Deegan *et al*. have experimentally investigated rapid fracture in rubber sheets by stretching a rubber sheet in biaxial directions in air. They found that a transition from straight to oscillatory cracks occurs under biaxial strain [2]. Moreover, they demonstrated that the transition is a Hopf bifurcation [3]. The wavy crack patterns and the transition were subsequently reproduced by numerical simulations using various models [4,5] and several possible factors were proposed for the instability, including hyperelasticity, viscoelasticity, and nonlocal elasticity. Since the experiment of Deegan *et al*., several works on fast crack propagation have been progressively performed and recent studies reveal the important role of nonlinear elasticity on crack dynamics [6–13]. However, the problem of the oscillating instability in fast crack propagation is still hard to tackle due to the difficulty in measuring rapid crack propagation and treating rapid crack dynamics with significant inertia.

In contrast, as a different example of wavy cracks, Yuse and Sano reported instabilities of crack patterns in quenched glass plates [14]. In their experiments thermal stress is locally applied to a glass plate under the control of the position where the thermal gradient is concentrated. Accordingly, the crack tip propagates together with the thermal field, i.e., the speed of the crack tip can be controlled externally. Pattern formation of this type of fracture of brittle materials in quasistatic limits is well investigated within the framework of linear elasticity using the local symmetry criterion for crack growth [15,16] .

For the understanding of the rupture of rubber, if we could perform an experiment in which the crack propagation speed is significantly reduced, as done in the glass plate experiment, it may be possible to reveal the nature of thin elastomers under fracture being separated from dynamical aspects such as sound propagation. In this paper we propose a different experiment for investigating fracture in thin rubber films. In the experiment a rubber film is ruptured on a viscous fluid layer. Consequently, the crack propagation speed is significantly reduced by the resistant stress from the layer. If the resistant stress is large enough compared to the inertial force per unit surface of the film, the crack propagates slowly compared to the speed of sound. In such a situation the inertial effects of the rubber become negligible and the system can be described by an overdamped parabolic type of equation. We call this third type of situation slow fracture. In the present experiments we observed oscillatory instability in crack propagation when the applied strain is less than a characteristic value. The transition from straight to oscillatory patterns occurs near a strain at which the highly nonlinear elasticity of the rubber sheet is initially observed. We thus expected that the nonlinear elasticity may be a key factor for crack instabilities rather than the inertial effect. To investigate this we performed numerical simulations based on the neo-Hookean model [19] that exhibited nonlinearity at large strains. A comparison of the results with those from a conventional linear elastic model revealed that the nonlinear elasticity is a critical factor in inducing oscillatory instabilities.

II. EXPERIMENT

Here we describe the experimental procedure. Figure 1 shows schematic representations of the system. First we prepared plastic cylindrical rods with smooth surfaces. We then coated the rod with highly viscous silicon oil (Centi-Stokes Visco Liquid, As One) to form a thin fluid layer around it. Next we pushed the rod into an inflated cylindrical rubber film (Qualatex 260Q natural rubber balloons, Pioneer Balloon Company) as shown in Fig. 1(a). At this point the rod was covered by a double-layered skin of rubber. We cut off both ends of the rubber film and removed the outer skin so that a single-layered rubber film remained. In this way we made a film on a viscous fluid layer around the rod. It has stress-free boundaries at both ends and it can move in the axial direction under viscous resistance. In the circumferential direction the strain satisfies a periodic boundary condition. If the layer is very thin and the fluid is Newtonian, the resistant stress σ is described as $\sigma = (\eta/d)V$, where η is the viscosity of the oil, d is the thickness of the layer, and V is the sliding velocity of the film. Therefore we can utilize the viscous fluid layer to realize large η/d.

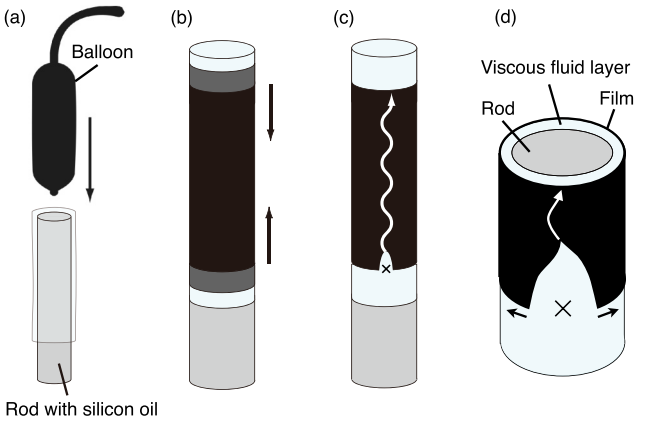

FIG. 1. (Color online) Schematic illustrations of the experimental procedure: (a) oil-coated cylinder covered by an inflated balloon, (b) relaxation to pure uniaxial tension, (c) crack initiation, and (d) cross section of the experimental system. The high-viscosity oil between the film and the rod significantly reduces the sliding speed of the film with respect to the substrate.

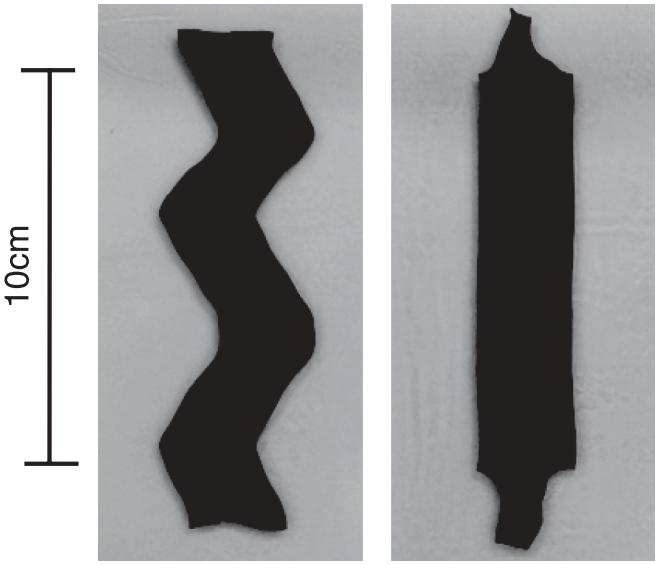

FIG. 2. Typical crack patterns in rubber films: oscillatory (left) and straight (right) crack patterns.

Just after the preparation of the sample, an unknown stress remains in the film. This residual stress causes the film to move in the axial direction on the rod to its elastic equilibrium state, i.e., pure uniaxial tension state, as shown in Fig. 1(b). According to observations, in the late stage of the relaxation, the film displacement decreases exponentially as a function of time, i.e., the end-to-end distance L of the film decays as $L \sim L_0 \exp(-t/\tau) + L_f$, where L_0 is the total shrinkage and L_f denotes the final length of the film in the relaxation. From an analysis of a uniform deformation of an elastic film on a viscous layer, the resistivity coefficient is estimated as

$$\frac{\eta}{d} \sim \frac{E\tau}{L_f},$$

where E is the Young modulus of the film. Therefore we are able to estimate the resistivity coefficient even without measuring d. Hereafter we use this relaxation time divided by the film length τ/L_f as an *indirect* control parameter of the experiments.

After equilibrium is attained, we initiate a small crack by cutting one end of the film in uniaxial tension as shown in Fig. 1(c). The crack starts to propagate if the initial strain is sufficiently large. The high oil viscosity significantly reduces the crack propagation speed. The crack speed typically lies in the range 0.01–1 m/s, which is much slower than that for a conventional balloon rupture. In this experiment the film drags the underlying oil so that the effective mass of the film increases, which may reduce the sound velocity of the film. We expect, however, that such an effect does not significantly change the sound speed of the film because the mass added by the oil is at most of the same order as the film itself. We also estimate that the order of viscous resistant stress is at least of the order of 10^3 Pa, while the inertial force per unit surface is 10^{-1} Pa. Therefore we can consider this system to be in an overdamped limit.

We repeated this procedure for various oil viscosities and rod diameters. To change the relaxation time we used silicon oils with viscosities in the range 1000–10 000 centistokes (cSt) and to change the applied strain we varied the rod diameter from 10 to 30 mm against the 20-mm natural circumferential width of the film. The balloons typically are 0.31 mm thick when they are unstretched.

In the experiments we observed two characteristic crack patterns: oscillatory patterns and straight patterns. Figure 2 shows typical examples of crack patterns [20]. Figure 3 shows a morphological phase diagram. Here strain refers to the nominal applied strain. Initial cracks do not propagate at strains less than a characteristic value ε_1. We observed oscillatory crack patterns when the applied strain exceeded ε_1. When the strain exceeded a critical value ε_2 in the large deformation regime, the crack path became straight. The propagation speed of the crack tip seems to increase linearly from the onset at ε_1, as shown in Fig. 3.

It should be noted that the critical strain ε_2 almost coincides with the characteristic strain at which the stress-strain relation of the rubber becomes nonlinear (see the stress-strain relation in Fig. 3). Here we have measured the stress-strain relation by weighting a piece of balloon in one direction. The stress is calculated by dividing the applied force by a deformed cross-section area perpendicular to the weighting direction and the deformed cross-section area is calculated by a uniaxial strain using an assumption of incompressibility. Because the balloon may have anisotropic elasticities due to its manufacturing process, we have measured the stress response in the longitudinal direction and circumferential direction of the balloon. As a result, there were no apparent dependencies on stretching direction.

Figure 4 shows the amplitude and the wavelength as functions of the applied strain. The quantities are nondimensionalized by the sample width (natural circumferential width) so we can compare them with simulation results in the following section. Below ε_2 both the oscillation amplitude and wavelength increase with decreasing applied strain. At the onset of oscillation ε_2, the wavelength remains finite (about

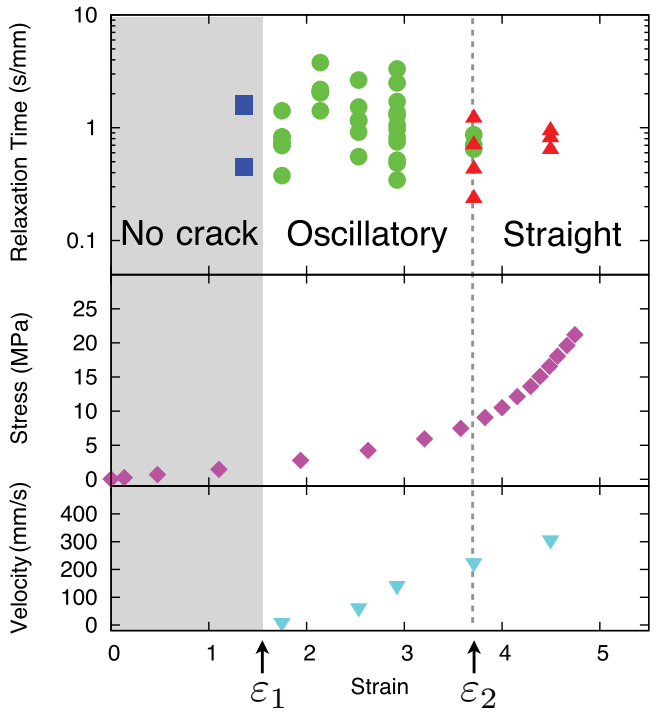

FIG. 3. (Color online) Experimentally obtained pattern diagram (top), stress-strain relation for rubber film (middle), and crack speed at each strain condition (bottom). The typical crack patterns observed are no crack (squares), an oscillatory crack (circles), and a straight crack (triangles). Relaxation time is normalized by the sample length L_f. In the regime in which the nonlinearity of the rubber becomes apparent, there is a transition from oscillatory to straight cracks. Crack speed is measured for the samples for which the relaxation time is approximately unity.

10 mm), whereas the amplitude becomes very small. This indicates that the transition may be a Hopf bifurcation [3]. Additionally, the large-amplitude oscillatory crack appears triangular. This Hopf-bifurcation-like behavior and triangular wave shape resemble those for a rapid fracture [2]. Large

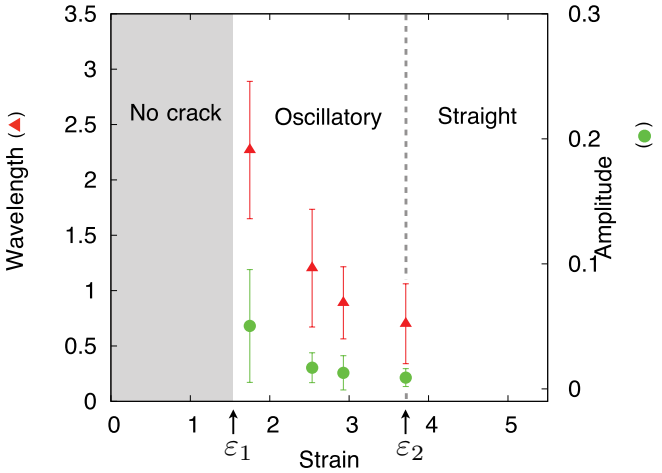

FIG. 4. (Color online) Dimensionless wavelength (triangles) and amplitude (circles) of an oscillatory crack against strain in units of the sample width. Values are averaged over different relaxation times, typically approximately 0.9 s/mm. The wavelength at the onset of the oscillation is nonzero.

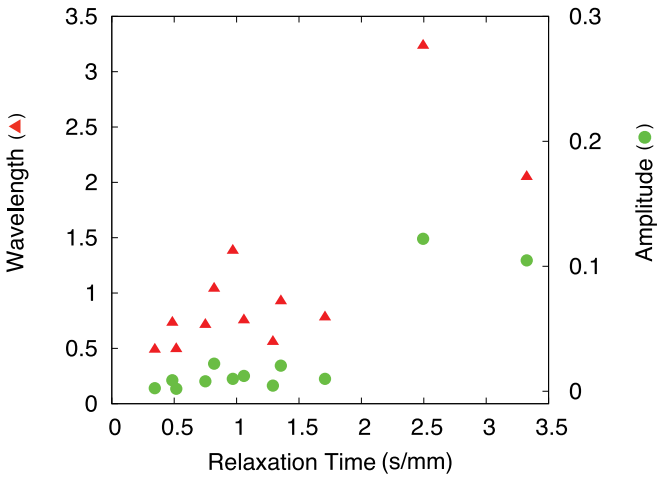

FIG. 5. (Color online) Dimensionless wavelength (triangles) and amplitude (circles) of an oscillatory crack against relaxation time in units of the sample width. The applied strain is 2.9.

scatters in the amplitude and the wavelength may be due to the inhomogeneity of the thickness of the balloon. The variation in thickness was about 20–30 %.

Furthermore, the amplitude and the wavelength are positively correlated with the relaxation time rescaled by the sample width under fixed strain conditions (Fig. 5). This tendency is characteristic in the present system of slow fracture. If the dynamics of this system was governed by a simple relaxation process of a purely elastic film accompanied by some resistive force, the length scales, such as the wavelength and amplitude of oscillation, should be decoupled from the relaxation time. To explain the dependence of characteristic length scales on the relaxation time as shown in Fig. 5, therefore, we need to introduce other dynamical effects, which include hysteresis, to introduce new length scales. For a more detailed analysis of pattern selection, it may not be possible to ignore other factors such as the viscoelasticity and plasticity of rubber. Figure 3 shows, however, that it seems those details do not change the stability of a crack pattern. Note that the dimensionless wavelength is always longer than approximately 0.5.

Based on the observation that the characteristic strain ε_2 is close to the onset of nonlinear elasticity of the rubber, we expect that the nonlinearity causes the pattern transition. We thus investigated whether this expectation is correct by performing numerical simulations under conditions with much fewer ambiguities.

III. NUMERICAL SIMULATIONS

We used the finite-element method with triangular elements to model a rubber film. We assumed that each triangular element was homogeneously deformed, i.e., the affine deformation, in which the strain in each element is determined by the relative positions of its vertices. The elastic properties of the elements are determined by the elastic energy function F assigned to them. In the present study we used two different energy functions: a neo-Hookean model, which has nonlinear elasticity, and a conventional linear elastic model [17–19].

For the neo-Hookean model the elastic energy is given by

$$F_i = \frac{1}{2}\mu\left(\lambda_{1i}^2 + \lambda_{2i}^2 + \frac{1}{\lambda_{1i}^2\lambda_{2i}^2} - 3\right)S_{0i}, \tag{1}$$

where λ_1 and λ_2 are the elongation ratios along the principal axes and S_0 is the area of the element in the resting state. The subscript i is used to denote quantities associated with the ith element. Since the neo-Hookean model has only a single adjustable parameter μ, one cannot independently adjust the elasticity coefficient and the characteristic strain of the model.

For the linear elastic model F_i is given by

$$F_i = \left[\frac{1}{2}\lambda\left(\sum_{j=1}^{2}\varepsilon_{jj}\right)^2 + \mu\sum_{j,k=1}^{2}\varepsilon_{jk}^2\right]S_{0i}, \tag{2}$$

where $\boldsymbol{\varepsilon}$ is the infinitesimal strain tensor. In Eqs. (1) and (2) λ and μ denote Lame constants; here we set them to $\lambda = 4$ and $\mu = 2$. Note that the two models coincide under infinitesimal deformation. We used the following criterion for the fracture condition: If the elastic energy density of an element $f_i = F_i/S_{0i}$ exceeds a critical value f_c, the element is permanently removed from the tiling.

To account for the viscous resistance the rubber sheet experiences, we introduced a dissipation function G defined as

$$G_i = \frac{1}{2}\gamma\int\left(\frac{d\boldsymbol{x}}{dt}\right)^2 dS_i, \tag{3}$$

where $\boldsymbol{x}$ is the position vector of a point in the ith element. The integral symbol $\int(\cdot)dS_i$ indicates that the integral is taken over all material coordinates of the ith element. Equation (3) implies that each point $\boldsymbol{x}$ in the element experiences a resistive force $-\gamma\dot{\boldsymbol{x}}$, where γ is the friction coefficient, which corresponds to the resistivity coefficient of the viscous resistance from the oil. Since we assumed the affine deformation in each element, G_i is represented by only the positions of the vertices of the triangular elements and its time derivatives.

Using the above F_i and G_i we can construct equations of motion for the positions of the vertices as

$$\frac{\partial}{\partial q_j}\left(\sum_{i=1}^{N}F_i\right) + \frac{\partial}{\partial \dot{q}_j}\left(\sum_{i=1}^{N}G_i\right) = 0, \tag{4}$$

where N is the total number of elements and $\boldsymbol{q} = \{x_1, y_1, x_2, y_2, \ldots, x_N, y_N\}$, where $\{x_i, y_i\}$ are the position coordinates of the ith vertex. Note that the inertia terms have been omitted in Eq. (4) because we can consider the experimental system to be approximately in an overdamped limit.

After discretizing the equation of motion in time, we solved a set of implicit equations to obtain the vertex positions in the next time step. We chose a sufficiently small time step to ensure that at most one breakage event occurred per time step. We imposed the periodic boundary condition in the lateral direction. The initial strain was given by the ratio of the period of the boundary condition to the width of the sheet; just as in experiments the initial strain was given by the ratio of the circumferential length of the cylindrical rod to that of the rubber sheet. We created a notch as the initial condition.

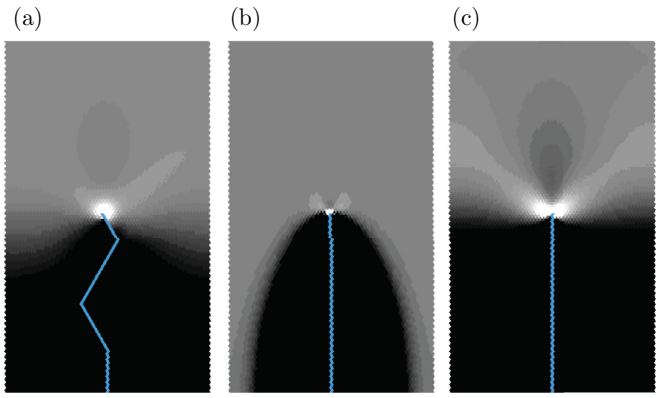

FIG. 6. (Color online) Typical crack patterns plotted with elastic energy density distributions obtained by simulations. The white regions represent regions with high elastic energies and the blue lines correspond to cracks. Positions are transformed into undeformed coordinates. Typical examples for a neo-Hookean model are (a) an oscillatory crack for an applied strain of $\varepsilon = 0.5$ and (b) a straight crack for an applied strain of $\varepsilon = 1.5$. With the linear elasticity model (c), only a straight crack is observed when the same strain was applied as for (a). The critical energy density is $f_c = 10$ in all examples. The number of elements is 128×256. Triangular elements are aligned such that one of the lattice vectors is parallel to the horizontal direction, which corresponds to the tensile direction.

The simulation results reveal that the crack morphology strongly depends on the nature of elasticity. Only the neo-Hookean model gave oscillatory patterns and the transition from a straight crack to an oscillatory crack. In contrast, the conventional linear model did not produce oscillatory cracks. Figure 6 shows typical crack patterns and elastic energy density distributions. Due to the discreteness of the triangular tiling, tiny oscillations are observed even for a straight pattern. In the neo-Hookean model, the high-energy region is more localized at the crack tip than in the linear elastic model and the region broadens with decreasing initial strain. In contrast, in the linear elastic model, the high-energy region is axisymmetric in the crack direction.

The morphology of the crack in the neo-Hookean model seems to depend on the nonlinearity of elastic response. Oscillatory patterns are observed for a strain below $\varepsilon_2 = 1.2$ for $f_c = 10$, where the nonlinear elasticity becomes apparent. In the region of larger strain, the neo-Hookean model gradually recovers the linear elasticity with larger elastic coefficients, which corresponds to the largely stretched rubber. For small strain, the crack patterns obtained depend on the threshold energy density f_c. When f_c is small enough but larger to sustain a single crack, as the applied strain increases, a straight crack appears first at the onset ε_1. In this case we could not observe oscillatory patterns even in the largely deformed regime. For large f_c, however, we observed oscillatory patterns when the applied strain exceeded a critical value ε_1; then there was a transition to straight patterns (at ε_2), just as in the experiments. Thus we can expect that the oscillation of a crack takes place for an intermediate magnitude of strain where the nonlinear elasticity becomes relevant for crack dynamics.

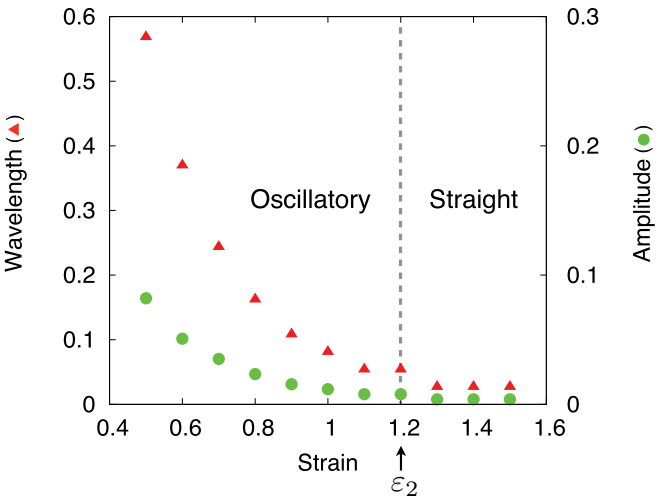

FIG. 7. (Color online) Dimensionless wavelength (triangles) and amplitude (circles) of an oscillatory crack against strain in units of the sample width for the neo-Hookean model. Due to the triangular tiling, there is a residual oscillation at short length scales even when a crack is straight on a macroscopic scale. The minimum strain required for crack propagation ε_1 is approximately 0.35.

For a comparison with the experiments we plotted the oscillation amplitude and wavelength versus applied strain (Fig. 7) near ε_2. Note that, due to the limited degree of freedom of the neo-Hookean model, the value of ε_2 was not adjusted to be consistent with the experimental results. In the simulations the oscillation wavelength and amplitude exhibited a proportional relationship and seemed to continuously decrease to zero with increasing applied strain. This result conflicts with the experimental results. Therefore, we do not have definitive evidence that the transition to oscillatory cracks can be described by a Hopf bifurcation. Further research is required to determine the details of the transition.

IV. CONCLUSION

In our experiments crack speed was reduced by a large resistant stress from the viscous fluid layer. If the resistivity is small enough compared to that of our experiments, a crack can propagate as rapidly as the speed of sound, where the dynamics is governed by a kind of hyperbolic differential equation. This situation is almost equivalent to the rapid fracture experiment done by Deegan *et al.* [2]. In such a rapid fracture, biaxial tension is considered to be an important condition to have oscillatory cracks [1]. In contrast, in the present study we found that oscillatory patterns are observed under uniaxial tension in both experiments and numerical simulations. Our results indicate that nonlinear elasticity is a key factor for oscillating crack paths in the case of a slow crack.

As another origin of oscillating cracks seen in thin elastic materials, it has been reported that out-of-plane motion plays a crucial role in the crack path [21]. In the present experiment there may be some out-of-plane motion because of the soft substrate; the effects of the increased freedom of motion of the film should be carefully investigated in the future. However, we believe that such out-of-plane motion is not primarily relevant to the oscillatory instability in our rubber film experiment because oscillatory cracks can be reproduced in pure two-dimensional simulations as well.

For a quantitative understanding of the present system, further investigation needs to be conducted. For example, the crack-tip speed and the magnitude of the critical strain $(\varepsilon_1,\varepsilon_2)$ and its dependence on the strength of the material (e.g., f_c) should be explained with a theory. From a dimensional analysis, the speed of the crack V should be described with the parameters of the model as

$$V \sim \frac{f_c^{(1-\xi)/2}\mu^{\xi/2}}{\gamma^{1/2}} F(\varepsilon),$$

where ξ is an unknown constant and F is a function. Unfortunately, in the current status, we have not performed a systematic survey, which makes the determination of the form of V possible mostly due to the limitation of computing time. As for ε_1 and ε_2, we expect that one can utilize the conventional linear elastic fracture mechanics (LEFM). Even under the condition of a small deformation, the local strain of the film could be large at the crack tip and the effective elastic coefficient might become highly inhomogeneous. However, we expect that some of the scaling relationships known in LEFM, such as $\varepsilon_1 \sim W^{-1/2}$, should still hold in the nonlinear case.

Another future work would be to study how the characteristic length and time of the oscillation are selected as well as the detailed origin of the oscillatory instability. When nonlinear elasticity becomes apparent, macroscopic length scales other than those in linear systems might appear. As seen in Fig. 6, the largely deformed region near the crack tip, which is brighter in the figure, changes in size and shape depending on the conditions. In the simulations of the neo-Hookean model we found that there is a robust tendency that the larger the spot size is, the larger the wavelength of oscillation becomes. We expect that such intrinsic length scales that arose from nonlinearity determine the characteristic length of the oscillation, which is essentially different from the quasistatic crack of linear brittle materials (e.g., in Refs. [14,15]) where the wavelength is primarily given by the sample width. In fact, in the studies of oscillatory instability in a rapid fracture [6–8], a similar statement had been proposed and checked by experiments and theory. They assert that the oscillation wavelength at the onset of the fast fracture instability is not determined by the size of the material, but determined by the material's intrinsic length, i.e., the length of the nonlinear zone near the tip. Slow fractures and the effect of the relaxation time on crack patterns are subjects for future research as there may be some coupling effects between the dynamics of the creep of the rubber sheet and the sliding on the cylinder that modify the crack patterns.

ACKNOWLEDGMENTS

We are grateful to Dr. T. Kawakatsu and Dr. N. Uchida for their helpful comments and suggestions. This work was supported by a Grant-in-Aid for Scientific Research (No. 21540377) from Ministry of Education, Culture, Sports, Science and Technology.

[1] A. Stevenson and A. Thomas, J. Phys. D **12**, 2101 (1979).
[2] R. D. Deegan, P. J. Petersan, M. Marder, and H. L. Swinney, Phys. Rev. Lett. **88**, 014304 (2001).
[3] See, e.g., J. Guckenheimer and P. Holmes, *Nonlinear Oscillations, Dynamical Systems, and Bifurcations of Vector Fields* (Springer-Verlag, New York, 1983).
[4] H. Henry and H. Levine, Phys. Rev. Lett. **93**, 105504 (2004).
[5] W. Wang and S. Chen, Phys. Rev. Lett. **95**, 144301 (2005).
[6] A. Livne, O. Ben-David, and J. Fineberg, Phys. Rev. Lett. **98**, 124301 (2007).
[7] E. Bouchbinder, Phys. Rev. Lett. **103**, 164301 (2009).
[8] T. Goldman, R. Harpaz, E. Bouchbinder, and J. Fineberg, Phys. Rev. Lett. **108**, 104303 (2012).
[9] A. Livne, E. Bouchbinder, and J. Fineberg, Phys. Rev. Lett. **101**, 264301 (2008).
[10] A. Livne, E. Bouchbinder, I. Svetlizky, and J. Fineberg, Science **327**, 1359 (2010).
[11] E. Bouchbinder, A. Livne, and J. Fineberg, Phys. Rev. Lett. **101**, 264302 (2008).
[12] E. Bouchbinder, A. Livne, and J. Fineberg, J. Mech. Phys. Solids **57**, 1568 (2009).
[13] E. Bouchbinder, Phys. Rev. E **82**, 015101(R) (2010).
[14] A. Yuse and M. Sano, Nature (London) **362**, 329 (1993).
[15] M. Adda-Bedia and Y. Pomeau, Phys. Rev. E **52**, 4105 (1995).
[16] E. Bouchbinder, H. G. Hentschel, and I. Procaccia, Phys. Rev. E **68**, 036601 (2003).
[17] L. D. Landau and E. M. Lifshitz, *Theory of Elasticity* (Butterworth-Heinemann, Oxford, 1986).
[18] A. Mal and S. Singh, *Deformation of Elastic Solids* (Prentice-Hall, Englewood Cliffs, NJ, 1991).
[19] M. Mooney, J. Appl. Phys. **11**, 582 (1940).
[20] See Supplemental Material at http://link.aps.org/supplemental/10.1103/PhysRevE.86.016106 for movie on crack patterns.
[21] B. Audoly, P. M. Reis, and B. Roman, Phys. Rev. Lett. **95**, 025502 (2005).